Applied Physics Letters

High performance ultraviolet photodetectors based on ZnO nanoflakes/PVK heterojunction

Cite as: Appl. Phys. Lett. **109**, 073103 (2016); https://doi.org/10.1063/1.4961114
Submitted: 09 June 2016 . Accepted: 04 August 2016 . Published Online: 15 August 2016

Yuhua Cai, Libin Tang, Jinzhong Xiang, Rongbin Ji, Sin Ki Lai, Shu Ping Lau, Jun Zhao, Jincheng Kong, and Kai Zhang

High performance ultraviolet photodetectors based on ZnO nanoflakes/PVK heterojunction

Yuhua Cai,[1] Libin Tang,[2,a)] Jinzhong Xiang,[1,b)] Rongbin Ji,[2,c)] Sin Ki Lai,[3] Shu Ping Lau,[3] Jun Zhao,[2] Jincheng Kong,[2] and Kai Zhang[4]
[1]*School of Physical and Astronomy, Yunnan University, Kunming 650091, People's Republic of China*
[2]*Kunming Institute of Physics, Kunming 650223, People's Republic of China*
[3]*Department of Applied Physics, The Hong Kong Polytechnic University, Hung Hom, Kowloon, Hong Kong*
[4]*Suzhou Institute of Nano-Tech and Nano-Bionics (SINANO), Chinese Academy of Science, Suzhou 215123, People's Republic of China*

(Received 9 June 2016; accepted 4 August 2016; published online 15 August 2016)

A high performance ultraviolet (UV) photodetector is receiving increasing attention due to its significant applications in fire warning, environmental monitoring, scientific research, astronomical observation, *etc*. The enhancement in performance of the UV photodetector has been impeded by lacking of a high-efficiency heterojunction in which UV photons can efficiently convert into charges. In this work, the high performance UV photodetectors have been realized by utilizing organic/inorganic heterojunctions based on a ZnO nanoflakes/poly (N-vinylcarbazole) hybrid. A transparent conducting polymer poly(3,4-ethylene-dioxythiophene):poly(styrenesulfonate)-coated quartz substrate is employed as the anode in replacement of the commonly ITO-coated glass in order to harvest shorter UV light. The devices show a lower dark current density, with a high responsivity (R) of 7.27×10^3 A/W and a specific detectivity (D^*) of 6.20×10^{13} cm $Hz^{1/2}/W^{-1}$ at 2 V bias voltage in ambient environment (1.30 mW/cm^2 at $\lambda = 365$ nm), resulting in the enhancements in R and D^* by 49% and one order of magnitude, respectively. The study sheds light on developing high-performance, large scale-array, flexible UV detectors using the solution processable method. *Published by AIP Publishing.*
[http://dx.doi.org/10.1063/1.4961114]

Ultraviolet (UV) photodetectors (PDs) have a wide range of applications including space communication, nondestructive testing of materials in industry, flame warning, UV radiation monitoring in environment, and biological agent detection.[1] Compared with the UV PDs based on wide band gap inorganic semiconductors that widely adopt the structures of Schottky photodiodes[2,3] and metal-semiconductor-metal junctions,[4,5] where complicated fabrication processes are required, UV PDs based on organic semiconductors have the advantages in terms of the simplicity of fabrication, readily suitable for large scale production, and low cost.

In recent years, ZnO has been intensively studied due to its outstanding optical properties which render it suitable for optoelectronic applications. With a wide direct bandgap of 3.37 eV at room temperature, ZnO has been regarded as an excellent semiconducting material for UV detection. ZnO materials can be synthesized by pulsed laser deposition,[6] radio frequency sputtering,[7] vapor-liquid-solid growth,[8] *etc*. Recently, solution-processed ZnO has also been extensively studied because of the low cost and potential for large scale production. In photovoltaics, colloidal ZnO nanoparticles have been shown to form bulk heterojunctions with conjugated polymers, which can combine the advantages of the individual component.[9,10] However, UV detectors based on ZnO synthesized by wet chemical techniques usually show slow photoresponse because of the high density of defects and the effect of gas adsorption and desorption on the crystal surface.[11–13] Compared with the metal-semiconductor-metal structure that is commonly applied in those detectors,[11–13] *p-n* junction devices usually demonstrate obvious advantages over the former one in the high frequency domain.[1] For example, Mridha and Basak reported that the ZnO/polyaniline heterojunction possesses a faster photoresponse to UV light than the pristine ZnO.[14] In this letter, we fabricated ZnO nanoflakes (NFs)/poly (N-vinylcarbazole) (PVK) hybrid devices, in which ZnO acts as an electron acceptor and electron transport material; PVK acts as an electron donor and hole transport material, in order to explore the feasibility of realizing fast UV photoresponse based on the solution-processed heterojunction devices. Although UV detectors applying polyfluorene (PFO) and ZnO nanorod arrays with good performance were recently reported,[15] ZnO nanoparticles employed in this work can further increase the interfacial area between the two hybrid components. Since an internal electric field exists at the interface of the hybrid, the increase in the interfacial area can allow more excitons generated under irradiation to diffuse into the interface before recombination and subsequently dissociate into free carriers.[9,10] In addition, this work demonstrates that the anode using the conducting polymer poly(3,4-ethylene-dioxythiophene):poly(styrenesulfonate) (PEDOT:PSS) is especially suitable for UV photodetectors owing to its high transmittance in the UV region, and it has excellent electrode properties such as high electrical conductivity, solution processability, and good stability in elevated temperature.[16–18]

In this paper, we fabricated the high performance ZnO NFs/PVK hybrid UV photovoltaic detector. The optical,

a)E-mail: scitang@163.com
b)E-mail: jzhxiang@ynu.edu.cn
c)E-mail: jirongbin@gmail.com

electrical, and photoelectrical properties of ZnO NFs/PVK as a photodetector have been systematically investigated to uncover the underlying mechanism of the strong photoresponse.

Poly(N-vinylcarbazole) (99.5%) was purchased from Beijing Aglaia Technology Development Co., Ltd. Zinc acetate dihydrate (99%) was purchased from Tianjin BoDi Chemical Co., Ltd. PEDOT:PSS was purchased from Sigma-Aldrich. All the chemical reagents were used without further purification.

The preparation of ZnO nanoflakes was similar to that of the ZnO nanorods which had been described previously.[19] Briefly, zinc acetate dihydrate (1.475 g) was dissolved in methanol (62.5 ml) under stirring at 60 °C in a reflux apparatus. Afterwards, a solution of KOH (0.188 g) dissolved in methanol (65 ml) was injected drop-wise for 45 min. After refluxing for 5 h at 60 °C, the reaction was quenched by cooling down the solution to room temperature and then was left in a static condition for two weeks. To precipitate out the ZnO, 60 ml of supernatant methanol was removed and replaced by fresh methanol. After repeated stirring and precipitation, the product was centrifuged at 2500 rpm. The isolated precipitate was dissolved in chloroform, using a 1:3 weight ratio of chloroform and ZnO precipitate. The as-obtained colloidal solution of ZnO NFs was translucent and had a high concentration of about 120 mg/ml. The solution was further diluted by adding a binary mixture of chloroform and ethanol (3:1 volume ratio) under stirring.

The UV organic photodetectors (OPDs) investigated in this work adopted a structure of Al/ZnO NFs/PVK/PEDOT:PSS(buffer layer)/PEDOT:PSS(anode)/quartz. The fabrication process is schematically shown in Fig. 1(a).The quartz substrate was pre-cleaned in an ultrasonic bath with ethanol, acetone, and deionized water for 15 min sequentially. Before fabrication, a highly conductive PEDOT:PSS (CLEVIOS PH1000) used as the anode layer was prepared according to the method described previously.[20] PVK was dissolved in chloroform with a concentration of 10 mg/ml and the solution was spin-coated onto the PEDOT:PSS buffer layer at 2500 rpm; then, the films were baked in a vacuum oven for 1 h at 100 °C. ZnO NFs (120 mg/ml) were spin-coated onto PVK at 1500 rpm. Then, films were baked in a vacuum oven for 2 h at 80 °C. The Al cathode was subsequently deposited onto the ZnO layer by thermal evaporation through a shadow mask at a pressure of 8.2×10^{-5} Pa. The thickness of the Al cathode was 110 nm, which was monitored by a quartz oscillator during deposition and the deposition rate was controlled at 2.5 nm/s. The effective area of the devices was 4.0 mm^2.

Control devices with the structure Al/ZnO NFs/PVK/PEDOT:PSS(buffer layer)/ITO/glass were also fabricated, which have the same structure as the devices mentioned above, except that the PEDOT:PSS anodes were replaced by the conventional ITO glasses to compare the UV detecting performance. The control devices were designated as ITO-device throughout the manuscript. The structure of the ITO-device is schematically shown in Fig. S1 in the supplementary material.

To investigate the performance of the ZnO NFs/PVK hybrid in UV detection, the vertical photovoltaic detectors have been fabricated with the procedure described in detail above. The cross-sectional image of the device was

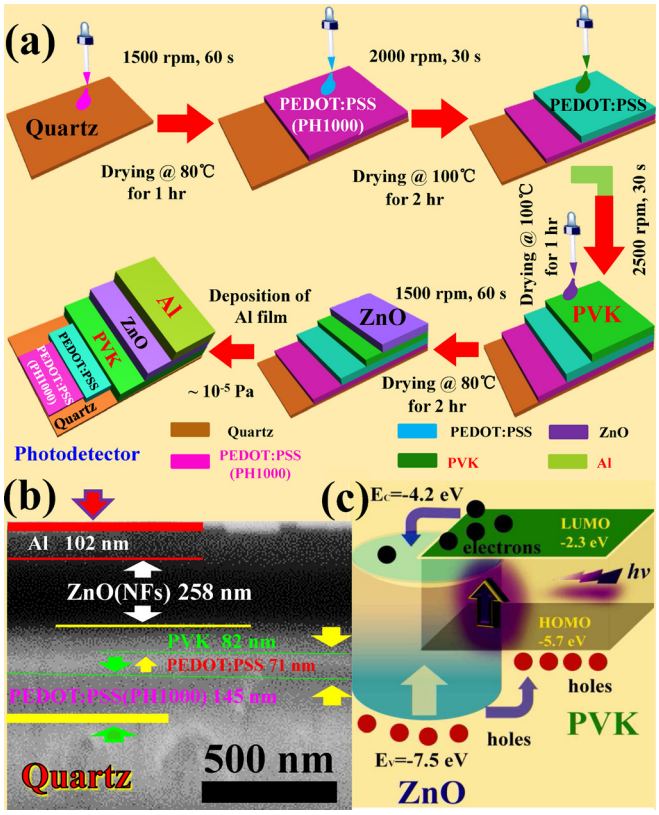

FIG. 1. (a) Schematic diagram illustrating the fabrication process of the UV photovoltaic detectors. (b) The SEM cross-sectional image of the detector, scale bar: 500 nm. (c) The energy level diagram of the ZnO NFs/PVK hybrid.

characterized by a scanning electron microscope (SEM, Hitachi S-3400N) as shown in Fig. 1(b). From the figure, the thicknesses of each layer in the device can be estimated. The PEDOT:PSS layer, used as the buffer layer in the control device, was 71 nm thick. The active layer consisting of PVK and ZnO NFs is of 82 nm and 258 nm thick, respectively. The energy level diagram of the hybrid is illustrated in Fig. 2(c). PVK is known for its high hole mobility, despite the fact that it is not a conjugated polymer, and has a wide bandgap.[21] Due to the large overlap in the UV absorption region between PVK and the ZnO NFs, the PVK layer acts not only as the hole transport layer but also as the UV absorbing layer.[15] The photo-generated electron–hole pairs are produced in both the ZnO NFs and PVK layers under the illumination of UV light. The holes in the ZnO NFs migrate from the valence band (VB) of ZnO to the HOMO of PVK due to the offset between the HOMO of PVK (−5.7 eV)[22] and the VB of ZnO NFs (−7.5 eV),[23] while the electrons in PVK will migrate from the LUMO of PVK to the conduction band (CB) of ZnO NFs due to the offset between the CB of ZnO NFs (−4.2 eV) and the LUMO of PVK (−2.3 eV); the holes in the HOMO of PVK and the electrons in the CB of ZnO NFs would then be transported to and collected by the PEDOT:PSS anode and the Al cathode, respectively, and results in the observed photocurrent.

The interfacial morphology of the active layer plays an important role in optoelectronic devices. SEM has been used to investigate the morphology of ZnO NFs layer. Fig. 2(a) shows the SEM image of ZnO NFs on the quartz substrate

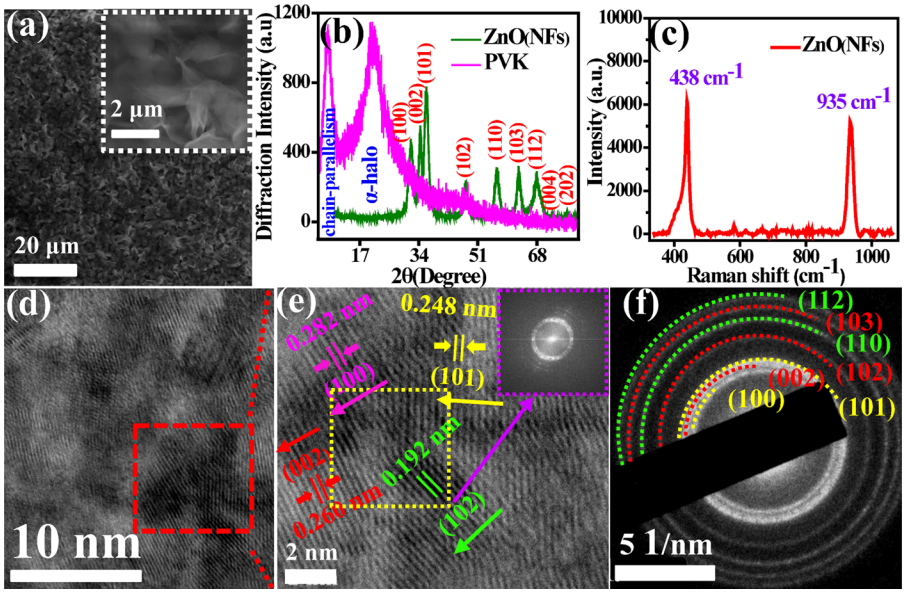

FIG. 2. (a) SEM image of ZnO NFs on quartz. The inset presents an enlarged image of the ZnO NFs. (b) XRD patterns of PVK and ZnO NFs. (c) Raman spectrum of the ZnO NFs. (d) The TEM image of ZnO NFs. (e) The HRTEM image of polycrystalline ZnO NFs and their selected area FFT pattern (inset). (f) Electron diffraction pattern of ZnO NFs with the expected wurtzite structure as indicated by the analysis shown in the figure.

which revealed the morphology of the nanoflakes in the product. The nanoflakes grew vertically on the substrate and formed an intertwined pattern. It can be seen from the magnified image of the ZnO NFs (inset of Fig. 2(a)) that each nanoflake consists of smaller nanoparticles. The sizes of nanoparticles are 15–20 nm which are stacked to produce the nanoflakes. The X-ray diffraction (XRD) pattern of ZnO NFs and PVK is shown in Fig. 2(b). Nine XRD peaks were observed in the pattern of the ZnO NFs, the corresponding lattice planes were labeled in the figure showing a wurtzite structure, which agrees well with the reported works.[24] These strong and wide peaks revealed that the obtained ZnO NFs have a good crystallinity in the nanoscale. The XRD pattern obtained from the PVK was similar to that reported previously.[25] Two diffraction peaks centered at $2\theta = 20.45°$ and 7.23° were observed with the corresponding d-spacing of 4.331 Å and 11.50 Å, respectively. The former peak ($2\theta = 20.45°$) was broad and diffuse, that was attributed to the amorphous halo, whereas the latter peak ($2\theta = 7.23°$) was attributed to the chain parallelism of PVK.

The Raman spectrum of ZnO NFs was recorded at ambient temperature using a Renishaw inVia Raman microscope with an argon-ion laser at an excitation wavelength of 514 nm. The spectrum is shown in Fig. 2(c). It can be seen from the figure that there are two dominating vibration peak centers at 438 and 935 cm^{-1}, respectively. The ZnO powders display a narrow and strong band at 438 cm^{-1} that has been assigned to E_2 mode, which arises from the motion of Zn atoms, and is a characteristic feature of the wurtzite phase. The envelope above 935 cm^{-1} can be attributed to the overtones and/or combination bands.[26] Figs. 2(d) and 2(e) show the TEM and the HRTEM images of the ZnO NFs, respectively. As illustrated in the figure, the d-spacings for the (100), (002), (101), and (102) planes are $d_{ZnO}{}^{100} = 2.82$ Å, $d_{ZnO}{}^{002} = 2.60$ Å, $d_{ZnO}{}^{101} = 2.48$ Å, and $d_{ZnO}{}^{102} = 1.92$ Å, respectively, which are consistent with the reported values.[27] The selected area fast Fourier transform (FFT) pattern of the ZnO NFs is shown in the inset of Fig. 2(e), which indicates a hexagonal wurtzite structure of the ZnO NFs. Fig. 2(f) shows the electron diffraction pattern of ZnO NFs, which also verified a wurtzite structure after assigning the diffraction pattern to the corresponding sets of lattice planes as shown in the figure.

The functional groups of the ZnO NFs/PVK hybrid were determined using Fourier transform infrared (FTIR) spectroscopy. The FTIR spectra of the PVK and ZnO NFs are presented in Fig. 3(a). The spectrum of the ZnO NFs showed a strong and broad absorption band at ~540 cm^{-1}, which arises from the stretching of the Zn-O bonds. This peak has been reported to be at ~480 cm^{-1} for bulk ZnO.[28] The peaks of all ZnO NFs samples have shifted evidently to higher wavenumbers as compared to the bulk ZnO, which is resulted from the decrease in size and the increase in zinc content[29] of the ZnO NFs. The peak at ~1341 cm^{-1} (CH_3) might be resulted from the solvent methanol. The characteristic band of PVK was consistent with that reported in the literature.[30] The broad absorption in the range of 3300 to 3700 cm^{-1} was ascribed to the existence of hydroxyl groups on the surfaces. Furthermore,

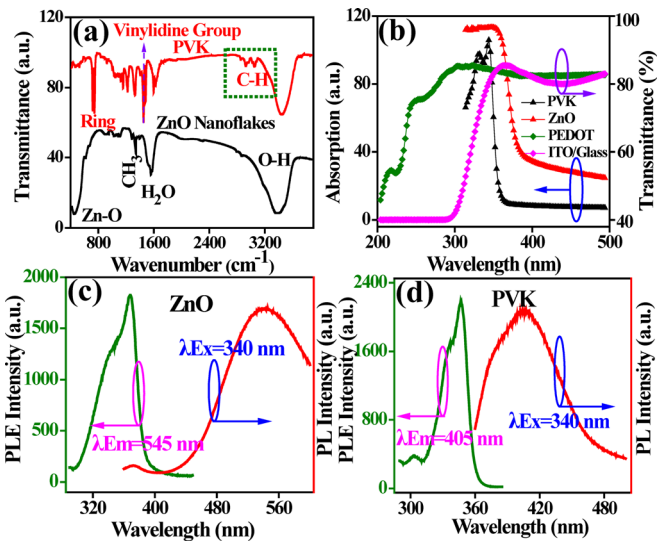

FIG. 3. (a) FTIR spectra of ZnO NFs and PVK. (b) The absorption spectra of ZnO NFs and PVK, and the transmission spectra of the ITO/glass and PEDOT:PSS(PH1000)/quartz. (c), (d) The photoluminescence (PL) and the PL excitation (PLE) spectra of ZnO NFs and PVK, respectively.

three absorption peaks in the range of 2885 to 3125 cm^{-1}, 1438 to 1445 cm^{-1}, and 1320 cm^{-1} were observed; these were ascribed to the C–H bonding. The strong absorption peak at ~1659 cm^{-1} was assigned to C–O bonding. The peak located at 740 cm^{-1} was attributed to the out-of-plane C–H deformation of the aromatic ring.[31]

Fig. 3(b) shows the UV-Vis absorption spectra of ZnO NFs and PVK. For PVK, a strong absorption band is observed between 320 and 350 nm, and there is no absorption for wavelength longer than 360 nm. The absorption spectrum of ZnO NFs shows a typical property for semiconductor, where a sharp absorption edge is located at 380 nm which corresponds to the interband transition. The transmission spectra of the ITO glass and PEDOT:PSS(PH100)-coated quartz are also shown in Fig. 3(b). It could be observed that the transmittance of ITO glass is about 80% for wavelength longer than 350 nm, but there is a sharp absorption for wavelength shorter than 350 nm and it is nearly opaque below 300 nm. Therefore, ITO glass is not suitable to be used in photodetectors designed for short wavelength UV light. On the other hand, the PEDOT:PSS-coated quartz substrate is basically transparent with a transmittance >93% in the UV region from 400 to 250 nm and is almost semi-transparent from 210 nm to 250 nm. The conducting polymer PEDOT:PSS is demonstrated to be an outstanding transparent electrode for organic UV PDs designed for short wavelength UV detection, as compared with the ITO-coated glass.

The PL spectra of ZnO NFs and PVK were recorded using an iHR-320 spectrometer and the results are shown in Figs. 3(c) and 3(d), respectively. The PL excitation (PLE) spectrum of ZnO NFs was recorded at an emission wavelength of 545 nm with the corresponding PLE peak located at 360 nm. The PLE spectrum of PVK was recorded at an emission wavelength of 405 nm with the PLE peaks located at 320 and 350 nm. For the PL emission spectra, an excitation wavelength of 340 nm has been used for both ZnO NFs and PVK samples, and the emission peaks for ZnO NFs are centered at 545 nm, while that for PVK is centered at 405 nm, as shown in Figs. 3(c) and 3(d), respectively.

In order to evaluate the performance of the device, the detector was illuminated with 365 nm UV light under a series of illumination intensities of 0.01, 0.06, 0.40, and 1.30 mW/cm^2 sequentially. Light passed from the PEDOT:PSS(PH100)/quartz side. The *J–V* characteristic and the logarithmic *J–V* curves of the devices with PEDOT:PSS anodes are shown in Figs. 4(a) and 4(b), respectively. It can be seen that on the whole, the photocurrent density increases with increasing light intensity ($\lambda = 365$ nm); this may be resulted from the fact that the absorbed light in photoactive material increases and more photogenerated carriers are produced at higher light intensity.

The effects of illumination intensity and bias voltage on the responsivity are shown in Fig. 4(c).The responsivity (R) is related to the photocurrent (I_{Ph}) by the relation, $R = I_{Ph}/W$, where W is the optical power received over the effective area of the device. It can be clearly seen that at a fixed bias voltage, the responsivity decreases with illumination intensity. On the other hand, the detector shows a higher responsivity at a larger bias voltage for a fixed light intensity. A responsivity as high as 7.27×10^3 A/W has been reached at 2 V bias voltage under an illumination intensity of 1.30 mW/cm^2, while

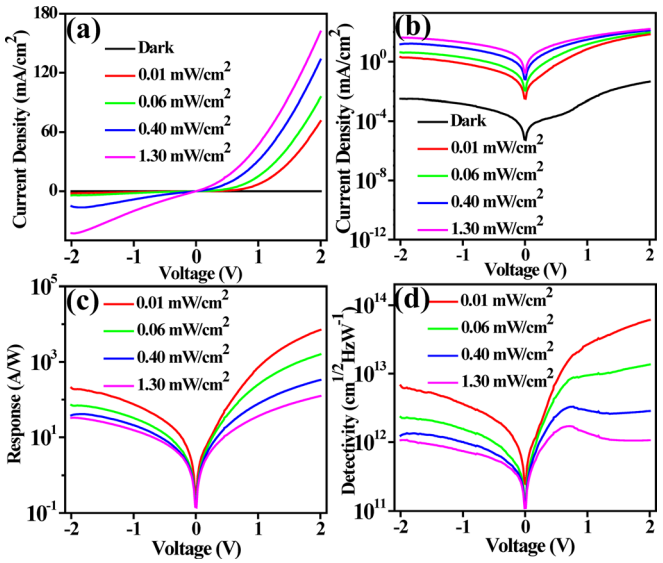

FIG. 4. (a) *J–V* characteristic curves and (b) the log *J–V* plot of the devices with PEDOT:PSS anodes under different illumination intensities at 365 nm. Variations of (c) the responsivity and (d) the detectivity with bias voltage and illumination intensities of the ZnO NFs/PVK-based UV photodetectors.

the ITO-device showed a responsivity of 4.89×10^3 A/W under the same light intensity as shown in the supplementary material. Thus, it demonstrated that the devices with PEDOT:PSS anode show a 49% increase in responsivity over the devices with ITO anode at 365 nm.

Detectivity (D^*) is an important parameter characterizing the normalized signal-to-noise performance of the photodetectors. Since the shot noise from the dark current is the major contribution to the noise of the detectors, D^* may be calculated using the following equation:[32,33] $D^* = R/(2qJd)^{1/2}$, where R is the responsivity, q is the electron charge (1.6×10^{-19} C), and J_d is the dark current density. The detectivity of the ZnO NFs/PVK-based detector is voltage-dependent as shown in Fig. 4(d). The highest detectivity is obtained at 2 V, with a value of 6.20×10^{13} cm $Hz^{1/2}$ W^{-1}. This value is comparable to that of the inorganic GaN, ZnO, Si photodetectors and other previously reported UV OPDs.[34,35] In comparison, the detectivity of the ITO-device reached 5.61×10^{12} cm $Hz^{1/2}$ W^{-1} under the same condition as shown in the supplementary material. Therefore, the detectivity of the devices with PEDOT:PSS anode is one order of magnitude higher than that for the devices with ITO anode.

The time response of the ZnO NPs/PVK-based UV detector has been measured as shown in Fig. S4. The rise and decay times are obtained by fitting the transient response with $I_r(t) = I_{r0} + A_r \exp(t/\tau_r)$ and $I_d(t) = I_{d0} + A_d \exp(-t/\tau_d)$, where τ_r and τ_d are the rise and decay time constants, respectively. The fitting results gave a rise time of $\tau_r = 0.902$ s and a decay time of $\tau_d = 1.202$ s.[36] A ratio of the current under illumination to the dark current is as high as ~10^4, which is obtained when irradiated by 365 nm LED with an intensity of 1.30 mW/cm^2 under the reverse bias. Our results show that the ZnO NFs/PVK hybrid device with PEDOT:PSS anode is very promising for high-performance UV photovoltaic detectors.

In conclusion, a high performance UV PD based on ZnO NFs and PVK with the transparent conducting polymer

PEDOT:PSS anode was fabricated. The highest detectivity (D^*) reaches 6.20×10^{13} cm $Hz^{1/2}$ W^{-1} and a responsivity as high as 7.27×10^3 A/W has been reached at 2 V bias voltage under 365 nm illumination with an intensity of 1.30 mW/cm^2 at ambient condition. This work demonstrates that the transparent conducting polymer PEDOT:PSS is a superior transparent electrode to the ITO glass for UV PDs. Due to the attractive solution-processable property of the ZnO NFs/PVK inorganic/organic UV photovoltaic detectors, the present study leads the way to developing high-performance, low-cost, and large-array UV photodetectors.

See supplementary material for the schematic diagram of device A (supplementary Figure S1), and the photovoltaic properties of device A (supplementary Figure S2), the power density of the UV LED ($\lambda = 365$ nm) as a function of supplied voltage (supplementary Figure S3), the comparison of the ZnO/PVK based UV detector fabricated in this paper with some common UV detectors (supplementary Table S1 and S2), and the time response of the ZnO/PVK based UV detector to light (supplementary Figure S4).

This work was supported by National Natural Science Foundation of China (Nos. 61106098 and 51201150), and the Key Project of Applied Basic Research of Yunnan Province, China (No. 2012FA003).

[1]M. Razeghi and A. Rogalski, J. Appl. Phys. **79**, 7433 (1996).
[2]M. Liao, Y. Koide, and J. Alvarez, Appl. Phys. Lett. **88**, 033504 (2006).
[3]R. Dahal, T. M. Al Tahtamouni, Z. Y. Fan, J. Y. Lin, and H. X. Jiang, Appl. Phys. Lett. **90**, 263505 (2007).
[4]G. Mazzeo, G. Conte, J. L. Reverchon, A. Dussaigne, and J. Y. Duboz, Appl. Phys. Lett. **89**, 223513 (2006).
[5]J. Li, Z. Y. Fan, R. Dahal, M. L. Nakarmi, J. Y. Lin, and H. X. Jiang, Appl. Phys. Lett. **89**, 213510 (2006).
[6]X. G. Zheng, Q. S. Li, W. Hu, D. Chen, N. Zhang, M. J. Shi, J. J. Wang, and L. C. Zhang, J. Lumin. **122**, 198 (2007).
[7]K. W. Liu, J. G. Ma, J. Y. Zhang, Y. M. Lu, D. Y. Jiang, B. H. Li, D. X. Zhao, Z. Z. Zhang, B. Yao, and D. Z. Shen, Solid-State Electron. **51**, 757 (2007).
[8]C. L. Hsu, S. J. Chang, Y. R. Lin, P. C. Li, T. S. Lin, S. Y. Tsai, T. H. Lu, and I. C. Chen, Chem. Phys. Lett. **416**, 75 (2005).
[9]W. J. E. Beek, M. M. Wienk, and R. A. J. Janssen, Adv. Funct. Mater.**16**, 1112 (2006).
[10]W. J. E. Beek, M. M. Wienk, M. Kemerink, X. N. Yang, and R. A. J. Janssen, J. Phys. Chem. B **109**, 9505 (2005).
[11]S. E. Ahn, H. J. Ji, K. Kim, G. T. Kim, C. H. Bae, S. M. Park, Y. K. Kim, and J. S. Ha, Appl. Phys. Lett. **90**, 153106 (2007).
[12]R. Ghosh, M. Dutta, and D. Basak, Appl. Phys. Lett. **91**, 073108 (2007).
[13]Y. Z. Jin, J. P. Wang, B. Q. Sun, J. C. Biakesley, and N. C. Greenham, Nano Lett. **8**, 1649 (2008).
[14]S. Mridha and D. Basak, Appl. Phys. Lett. **92**, 142111 (2008).
[15]Y. Y. Lin, C. W. Chen, W. C. Yen, W. F. Su, C. H. Ku, and J. J. Wu, Appl. Phys. Lett. **92**, 233301 (2008).
[16]S. K. Hau, H. L. Yip, J. Zou, and A. K. Y. Jen, Org. Electron. **10**, 1401–1407 (2009).
[17]Y. S. Kim, S. B. Oh, J. H. Park, M. S. Cho, and Y. K. Lee, Sol. Energy Mater. Sol. Cells **94**, 471–477 (2010).
[18]M. Girtan and M. Rusu, Sol. Energy Mater. Sol. Cells **94**, 446–450 (2010).
[19]C. Pacholski, A. Kornowski, and H. Weller, Angew. Chem., Int. Ed. **41**, 1188 (2002).
[20]L. Zhu, W. S. Wang, Z. G. Yao, X. Q. Zhang, and Y. S. Wang, Solid-State Electron. **80**, 14 (2013).
[21]F. Guo, B. Yang, Y. Yuan, Z. Xiao, Q. Dong, Y. Bi, and J. Huang, Nat. Nanotechnol. **7**, 798 (2012).
[22]X. H. Yang, F. Jaiser, B. Stiller, D. Neher, F. Galbrecht, and U. Scherf, Adv. Funct. Mater. **16**, 2156 (2006).
[23]N. Tokmoldin, N. Griffiths, D. D. Bradley, and S. A. Haque, Adv. Mater. **21**, 3475 (2009).
[24]F. Zhang, L. D. Sun, and C. H. Yan, Chem. Phys. Lett. **422**, 46–50 (2006).
[25]Y. Chen, R. F. Cai, L. X. Xiao, Z. E. Huang, and D. Pan, J. Mater. Sci. **33**, 4633 (1998).
[26]U. Ozgur, Y. I. Alivov, C. Liu, A. Teke, M. A. Reshchikov, S. Dogan, V. Avrutin, S. J. Cho, and H. Morkoc, J. Appl. Phys. **98**, 041301 (2005).
[27]R. Buonsanti, A. Llordes, S. Aloni, B. A. Helms, and D. J. Milliron, Nano Lett. **11**, 4706–4710 (2011).
[28]N. Vigneshwaran, S. Kumar, A. A. Kathe, P. V. Varadarajan, and V. Prasad, Nanotechnology **17**, 5087 (2006).
[29]A. Dev, R. Niepelt, J. P. Richters, C. Ronning, and T. Voss, Nanotechnology **21**, 065709 (2010).
[30]T. Chen, G. Z. Xing, Z. Zhang, H. Y. Chen, and T. Wu, Nanotechnology **19**, 435711 (2008).
[31]P. Bertoncello, A. Notargiacomo, V. Erokhin, and C. Nicolini, Nanotechnology **17**, 699 (2006).
[32]X. Gong, M. H. Tong, Y. G. Xia, W. Z. Cai, J. S. Moon, Y. Cao, G. Yu, C. L. Shieh, B. Nilsson, and A. J. Heeger, Science **325**, 1665 (2009).
[33]L. T. Dou, Y. M. Yang, J. B. You, Z. Hong, W. H. Chang, G. Li, and Y. Yang, Nat. Commun. **5**, 5404 (2014).
[34]L. Zhu, Q. Dai, Z. F. Hu, X. Q. Zhang, and Y. S. Wang, Opt. Lett. **36**, 1821 (2011).
[35]H. Wu, W. L. Li, B. Chu, C. S. Lee, Z. S. Su, J. B. Wang, F. Yan, G. Zhang, Z. Z. Hu, and Z. Q. Zhang, Appl. Phys. Lett. **96**, 093302 (2010).
[36]C. Soci, A. Zhang, B. Xiang, S. A. Dayeh, D. P. R. Aplin, J. Park, X. Y. Bao, Y. H. Lo, and D. Wang, Nano Lett. **7**, 1003 (2007).